

R. MEŽIBRICKÝ\*#, M. FRÖHLICHOVÁ\*, A. MAŠLEJOVÁ\*\*

## PHASE COMPOSITION OF IRON ORE SINTERS PRODUCED WITH BIOMASS AS A SUBSTITUTE FOR THE COKE FUEL

### SKŁAD FAZOWY SPIEKÓW ŻELAZA WYTWORZONYCH Z DODATKIEM BIOMASY JAKO ZAMIENNIKA DLA KOKSU

The effort to minimize CO<sub>2</sub> emissions leads the existing integrated steel plants to implement alternative biomass-based fuels that dispose of equilibrium carbon balance. The fuel is a key factor in the iron ore sinter production, so it is essential to know its impact not just on mechanical properties of the finished sintered ore but also on the mineral composition as the mineral phases together determine all observed sinter properties. For this purpose the samples prepared by replacing a part of coke breeze with charcoal or walnut shell substitute were subjected to the observation under the light microscope, also using etching, to the phase identification by chemical EDX analysis on the scanning electron microscope and to the phase composition quantification by X-Ray diffraction analysis. The studied microstructure areas in the vicinity of the pores left by fuel grains were neither characterized by different phases nor by changed chemical composition of these phases even though mineral matter of the used fuels were substantially different in terms of the chemical composition. The only feature of the burned substitute fuels were ash particles arranged in characteristic shapes. The main reason of variation in ratios of respective mineral phases of samples appeared to be thermal conditions that were reflected in the content of unreacted non-ferrous phases. Coke substitution in the sinter mixture has no negative impact on the phase composition of the produced sinters, which confirms the prospective use of biofuels in the sintering process.

*Keywords:* ash, biomass, coke breeze, iron ore sinter, microstructure, mineral composition

Cel jakim jest zmniejszenie emisji CO<sub>2</sub> do atmosfery, skłania istniejące zintegrowane huty stali między innymi do wprowadzania alternatywnych paliw opartych na bazie biomasy. Paliwo jest kluczowym czynnikiem w produkcji spieku rud żelaza, dlatego istotna jest znajomość jego wpływu nie tylko na właściwości mechaniczne gotowego spieku, ale również na jego skład mineralogiczny. W ramach badań sporządzone próbki, w których część koksiku zastąpiono paliwem alternatywnym. Wytworzone spieki poddano obserwacji pod mikroskopem świetlnym, a także wykonano identyfikację faz za pomocą analizy EDX na skaningowym mikroskopie elektronowym. Ilościową analizę składu fazowego próbek wykonano poprzez dyfrakcyjną analizę rentgenowską. Zastąpienie części koksiku w mieszance spiekalniczej nie ma żadnego negatywnego wpływu na skład fazowy wytworzonych spieków, co potwierdza potencjalne wykorzystanie biopaliw w procesie spiekania.

## 1. Introduction

Most of the world steel production comes from integrated plants that use blast-furnace hot metal as an intermediate product. Despite a considerable expansion of pellets, today the iron ore sinter produced on sintering grates is still the most widely used ferrous part of the blast-furnace charge [1]. Since its origin, its production technology has undergone multiple innovations and now more and more attention begins to be paid to the progress in the area of reduction of negative impacts on the environment. One of the possibilities also is the implementation of fuels with equilibrium carbon balance during the combustion process, represented by the biomass [2]. Its main purpose is to reduce the CO<sub>2</sub> immision load of air, therefore it is considered to be a very prospective fuel.

Coke and different biomass-based fuel types have different

properties not only in terms of energy value but also from the point of view of physical nature or chemical composition. Depending on the pretreatment level, the biomass fuels have different contents of moisture, volatile substances and mineral matters [3-4], which have a significant impact on the sintering conditions. So far, the research in this area has shown that when replacing part of conventional fuel with biomass, it is possible to produce sinter without significant deterioration of the observed properties but a full substitution of coke breeze has not yet produced acceptable results [5-7].

All quality parameters of sinters are determined by the sum of properties of mineral phases of which they are composed. These phases can be divided by type into following four basic groups: iron oxides, calcium ferrites, silicates, and glass. In the past mainly acid sinters were produced, where calcium ferrites were present rather sporadically. The prerequisite for the

\* DEPARTMENT OF FERROUS AND FOUNDRY METALLURGY, TECHNICAL UNIVERSITY OF KOŠICE, LETNÁ 9, 042 00 KOŠICE, SLOVAK REPUBLIC

\*\* U. S. STEEL KOŠICE, S.R.O. VSTUPNÝ AREÁL U. S. STEEL, 044 54 KOŠICE, SLOVAK REPUBLIC

# Corresponding author: roland.mezibricky@tuke.sk

TABLE 1

Characteristics of the studied samples

	Standard sinter	Sinters with a substitute for part of fuel			
		Charcoal		Walnut shells	
Designation	A1	DU44	DU86	OS35	OS42
Fuel in the sinter mixture [wt %]	3.4	4.35	3.78	7.12	8.21
Coke substitute [wt %]	-	44	86	35	42

formation of calcium ferrites is basicity of the sinter mixture when the iron-ore gangue is mainly composed of  $\text{SiO}_2$ . As sinters assumed the role of the blast-furnace charge basicity regulators, they are generally produced with a substantial addition of CaO - based additives. Calcium ferrites thus became a common part of today's sinters while their type and ratio varies with increasing addition of basic additives [8-9].

The objective of the present paper is to evaluate the impact of used substitute fuels on the phase composition of sinters while taking into account the type and substitution level of the applied fuel.

## 2. Work methodology and materials

### 2.1. Sinter samples

The samples used for this study were taken from sinter cakes produced in the laboratory sinter pot. Its parameters and conditions obtained during the production are described in [10]. The sinter produced using a conventional fuel – coke breeze – served as a reference sample representing the standard composition of the sinter charge. In other cases a part of coke was replaced with alternative fuels of biomass - charcoal and walnut shells with the same grain size as was the coke breeze size. The replacement was performed based on energy values of fuels so that the fuel mixture heating value in each sinter charge corresponded to the reference sinter charge heating value. During the replacement with charcoal the amount of fuel changed only slightly in terms of weight ratio, but this does not apply to the replacement with walnut shells, the heating value of which is significantly lower compared to coke. It resulted in an increase in the fuel ratio in the sinter mixture up to 7.12 or 8.21 %. The characteristic of the samples is given in Table 1.

### 2.2. Methodology

The samples for the observation under the optical light microscope (LM) Olympus GX71 were prepared in such a way that they were embedded in epoxy resin and then grounded and polished. In order to prove or highlighting some phases the samples were etched with HCl,  $\text{HNO}_3$  or HF solutions. For using in the scanning electron microscope (SEM) with the Energy Dispersive X-ray Spectroscopy (EDX) function, a conductive Au-Pd mixture layer in the thickness of up to 1 nm was applied on the surface of the samples. As the semi-quantitative EDX analysis provides distorted values mainly for very light elements (C, O), a correction oxygen conversion

was necessary in some cases. Thereby the ratio of identified elements (except for oxygen) was converted to their oxides from which the stoichiometric ratio of oxygen was obtained. In case of calcium ferrites and ash, iron was taken into account in form of  $\text{Fe}_2\text{O}_3$ . Carbon values were recorded only for information.

The X-Ray diffraction analysis of finely-ground samples was carried out using the Seifert XRD 3003 PTS device, the measurement parameters are shown in Table 2. Diffraction records were analyzed by the DIFFRAC.EVA (Search-Match) software with the PDF2 database and the TOPAS software that uses the Rietveld method. Quality determination of phases in sinters respected the findings from the microscopic observations.

TABLE 2

X-Ray measurement parameters

Generator	35 kV, 40 mA
X-ray Radiation	Co - line focus
Filter	Fe
Scan step	0.02 theta
Range of measuring	10 - 130° 2theta
Input slits	3 mm, 2 mm
PSD detector	Meteor1D

## 3. Results and discussion

### 3.1. Sinters prepared using charcoal

It is appropriate to assess the effect of fuel on the phase composition by the microscopic observation in the vicinity of pores where individual grains of charcoal were burned. As the sinter bed is a very heterogeneous system, conditions for burning are different in almost every single part, which also results in an incomplete fuel oxidation. Unburned fuel particles relics identification makes it possible to compare the phase composition in their immediate vicinity.

An example of the coke grain residue embedded in the finished sinter material is shown in Figure 1. The walls of pores give an idea of the original grain size, obviously having a limited air supply during the sintering. It was undoubtedly also surrounded by the melt as all surrounding phases are the secondary ones – crystallizing from the melt. The EDX semi-quantitative analysis of this coke converted to oxides in mineral matter (Table 3) shows a clear prevalence of  $\text{Al}_2\text{O}_3$  that had along with  $\text{SiO}_2$  a major presence, in different ratios,

also in other found coke breeze residues. Such presence of components is in agreement with the general nature of coke the mineral components of which are of the strongly acidic nature [11]. The ratio of CaO in the coke mineral matter varies but normally it is very low. An independent coke study confirmed the presence of CaO in form of small grains that can this way locally increase its ratio in the chemical analysis, which is probably this case.

The matrix composed of anhedral silico-ferrites of calcium and aluminum (SFCA) with larnite crystals –  $\text{Ca}_2\text{SiO}_4$  can be clearly seen in the pore vicinity.

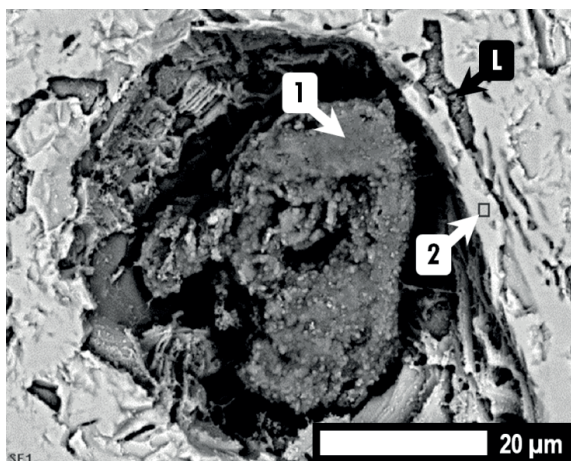


Fig. 1. Incompletely burned coke grain (SEM); L – larnite, 1, 2 – see Table 3

In contrary to coke, biomass-based fuel mineral matters are of the exactly opposite - basic nature that makes it possible to identify with sufficient accuracy the found relics of fuel grains by their chemical composition. Incompletely burned part of charcoal in Figure 2 has a high content of CaO (Table 3), which was a feature of all studied charcoal residues. It is interesting, that neither of them showed an increase ratio of potassium which has almost inherently a high ratio in the biomass mineral matters (~ 20 %) in form of  $\text{K}_2\text{O}$  [12]. On the contrary, there are visible increased concentrations of mainly  $\text{Fe}_2\text{O}_3$  and sometimes also  $\text{Al}_2\text{O}_3$ .

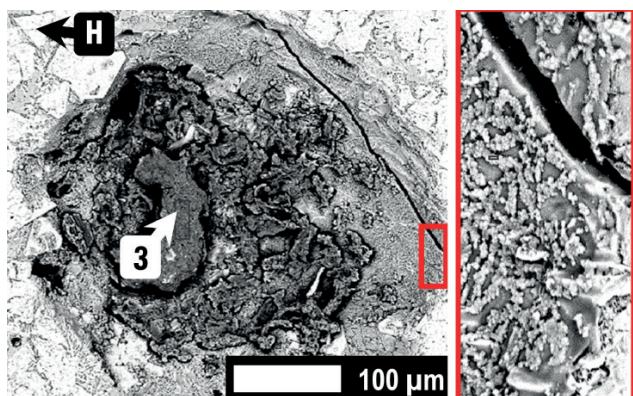


Fig. 2. The pore microstructure with a residue of charcoal and with a detail of the lime crystals (SEM); H – hematite, 3 – see Table 3

Some pores with the residues of charcoal had the walls covered with the cluster of crystalline chains as is shown in the section in Figure 2. From the chemical point of view these

are the particles of pure lime, which was confirmed by the performed EDX analysis. The substrate layer is amorphous phase with a clear glassy surface and a presence of calcium and silicon as well as iron. In this case there is no doubt that the found crystals are the immediate residue of the ash from the burned part of charcoal that was not integrated in the sinter material during the sintering process.

Phases crystallizing directly at the edges of the pore left by the burned charcoal are shown in Figure 3. In addition to the magnetite subhedral crystals, also thin SFCA plates intervene in the free space after the fuel burning. Although these thin plates contain potassium as well as sodium oxides, this is in the same time the only trace of alkali metals in the surrounding phases except the fuel residues (in the middle of pore). The phase composition of the displayed minerals corresponds to the phase composition of the wider environment of the pore, complemented with dicalcium silicates and dendritic formations of the secondary hematite.

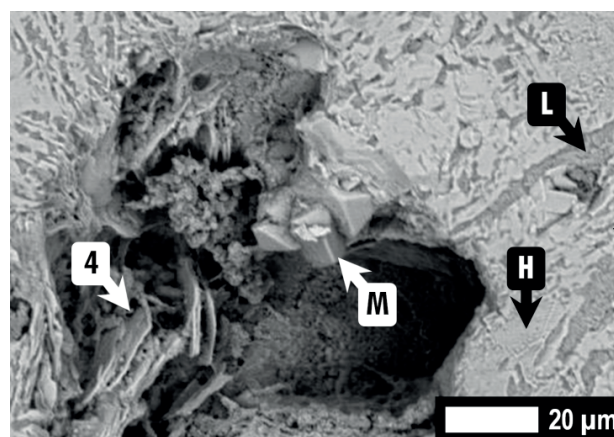


Fig. 3. Phase composition in the vicinity of the pore after the charcoal burning (SEM); M – magnetite, H – hematite, L – larnite, 4 – see Table 3

### 3.2. Sinters prepared using walnut shells

No conserved residues were found in the sinters produced using ground walnut shells, according to which it could be possible to distinguish their original cell structure. The found relics underwent an advanced oxidation and left in the sinter just ash and granular fragments. As in the case of charcoal, also in this case it was necessary to identify the residues by conversion to the composition of mineral matter. And this is very characteristic of the charcoal with a major ratio of CaO.

The microstructure of the pore left by the burned walnut shell fragment and its vicinity is shown in Figure 4. The characteristic network structure composed of thin fibers of mixed chemical composition can be clearly seen in the section (Table 3). It is a non-assimilated ash from walnut shells that maintained such unique form after the fuel flammable burning. Identical findings were revealed in case of most pores of this type. Ash distribution obviously reproduces the concentration of mineral matter in the solid fuel material. In addition, also independent small crystals of lime were observed, however without an arrangement in chains.

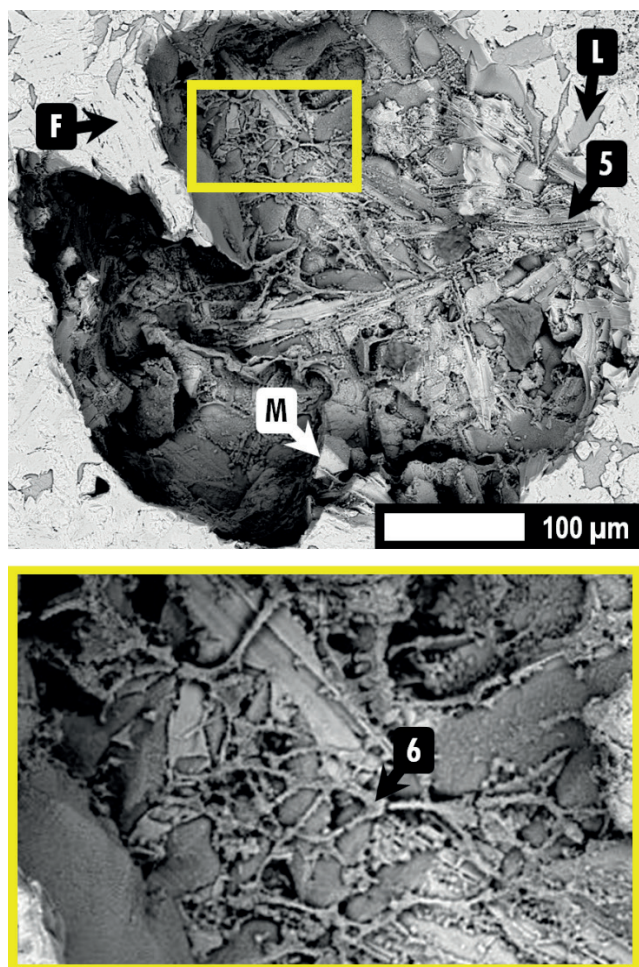


Fig. 4. The microstructure of the pore left by the burned walnut shell fragment (SEM); *F* – SFCA, *M* – magnetite, *L* – larnite, 5, 6 – see Table 3

The underlayer under the above-mentioned ash, shown in Figure 4 consists of lance-shaped  $\text{Ca}_2\text{SiO}_4$  crystals that are embedded in the surrounding material in the matrix composed of SFCA. The microstructure of these compounds features

thin plates combined in an integral tabular form, at the edges of which there are the CaO and ash particles. Based on these facts as well as on a preserved network form of ash it can be concluded that the crystallization of mineral phases was completed prior to the fuel total combustion.

Crystals of magnetite with a substitution of divalent iron  $\text{Fe}^{2+}$  with magnesium and calcium cations are still clearly visible between small SFCA plates as well as in the bottom part of the pore which is quite a common phenomenon in case of most similar crystals.

This implies that despite significant differences in the chemical composition of mineral matters of respective fuel types these differences did not manifest themselves in the phase composition even in the close vicinity of pores created after the fuel combustion. Besides the traces in silico-ferrites of calcium and aluminum, the increased content of the alkali metals oxides, the donor of which is the biomass ash, did not manifest itself in any way.

TABLE 3

EDX analysis of selected points after conversion to oxides

#	Oxide ratio [wt %]						
	$\text{Fe}_2\text{O}_3$	CaO	$\text{SiO}_2$	$\text{Al}_2\text{O}_3$	MgO	$\text{Na}_2\text{O}$	$\text{K}_2\text{O}$
1*	8.7	13.2	11.4	66.7	-	-	-
2	83.1	12.7	1.8	0.8	1.6	-	-
3*	14.1	49.6	13.3	17.5	4.5	1.1	-
4	67.5	19.1	9.4	1.9	1	0.5	0.6
5	83.2	12.8	2.2	1.1	0.8	-	-
6*	18.5	72.6	8.5	0.5	-	-	-

\* conversion to mineral matter (i.e. without carbon)

\*\* in the conversion all iron was considered as  $\text{Fe}^{3+}$ 

#### 4. Comparison of the phase composition of sinters

According to the performed X-Ray diffraction analysis, the phase composition of the studied sinters is the same, but

TABLE 4

Phase composition of sinters measured by the X-Ray diffraction analysis

Type	Phase	Formula	A1		DU44		DU86		OS35		OS42	
			[%]	Σ	[%]	Σ	[%]	Σ	[%]	Σ	[%]	Σ
iron oxides	hematite	$\text{Fe}_2\text{O}_3$	36.34	60.51	20.77	53.69	30.02	50.66	19.21	53.86	19.89	39.57
	magnetite	$\text{Fe}_3\text{O}_4$	23.81		32.43		20.16		34.29		19.29	
	wüstite	$\text{Fe}_{1-y}\text{O}$	0.36		0.49		0.48		0.36		0.39	
silicates	larnite	$\text{Ca}_2\text{SiO}_4$	6.60	14.16	7.22	16.96	7.44	14.06	10.72	19.52	10.19	19.67
	hedenbergite	$\text{CaFeSi}_2\text{O}_6$	6.49		8.34		4.94		6.31		7.40	
	wollastonite	$\text{CaSiO}_3$	1.07		1.40		1.68		2.49		2.08	
calcium ferrites	srebrodolskite	$\text{Ca}_2\text{Fe}_2\text{O}_5$	3.07	13.25	5.32	21.83	3.52	24.16	6.91	22.35	6.56	36.15
		$\text{Ca}_4\text{Fe}_9\text{O}_{17}$	2.35		3.91		3.96		3.81		4.72	
		$\text{CaFe}_5\text{O}_7$	1.70		3.21		5.01		6.11		7.53	
		$\text{Ca}_2\text{Fe}_{22}\text{O}_{33}$	5.12		8.79		9.32		5.00		16.34	
		brownmillerite	$\text{Ca}_2(\text{Al,Fe})_2\text{O}_5$		1.01		0.60		2.35		0.52	
non-assimilated non-ferrous phases	lime	CaO	-	11.23	-	6.54	-	8.57	1.85	4.29	2.45	4.60
	dolomite	$\text{CaMg}(\text{CO}_3)_2$	0.97		0.76		0.07		1.15		0.06	
	quartz	$\text{SiO}_2$	10.26		5.78		8.50		1.29		2.09	

the ratios of individual phases are different. Table 4 shows phases divided into groups by their type.

Within this division, when comparing the reference sinter to other sinters where an alternative fuel was used, there is a noticeable increase in the ratio of secondary phases – silicates and calcium ferrites and decrease in the ratio of primary phases – iron oxides and non-assimilated non-ferrous phases. When assuming preservation of a constant melting ability of materials, this phenomenon can be in all cases attributed only to increased temperatures in the sinter bed.

When considering the impact of the chemical composition of ash from burned fuels on the formation of secondary phases, it is important to take into consideration their concentration in the sinter mixture. Coke breeze itself is present in the sinter bed in very small amounts, so it cannot, even at high ash content, provide enough mineral components for formation of new phases.

When replacing a certain proportion with charcoal the total amount of fuel does not change very much, a low content of mineral matter in the charcoal, frequently not achieving even half of the value for coke, but it causes a decrease in the amount of minerals brought by ash.

When using walnut shells - that represent crude biomass - as a substitute material, the fuel mass percentage in the charge will increase significantly but the amount of brought mineral components for the alternative fuel minimum ash content will not increase.

Based on the above as well as on examination of the vicinity of found fuel residues it can be stated that even significant changes in the chemical composition of ashes do not cause the formation of different types of phases in the sinter.

#### 4.1. Non-assimilated non-ferrous phases

So, mainly different thermal conditions in the sinter bed can explain changes in the percentage of phase groups. These basically reproduce the percentage of residual phases, but mainly the content of quartz that can be considered as the indicator of assimilation rate of the sinter ore where it is the main part of the gangue.

SiO<sub>2</sub> is not present in the finished sinter in the secondary form. After its transition in the melt it always participates in the formation of other phases and crystallizes as a part of their lattice or remains in amorphous form, most frequently associated with CaO and FeO.

In addition to quartz, the group of non-assimilated non-ferrous phases also includes dolomite the unreacted white grains of which were a significant feature of the macrostructure of all studied sinters. A typical view of non-assimilated grain of dolomite with a phase interface with the surrounding material of sinter after etching with HCl is shown in Figure 5. The iron-rich melt penetrating into the volume of dolomite most frequently along the boundaries of its grains crystallizes in form of dicalcium ferrite that is a matrix for the dispersed periclase. The latter remains virtually in a pure form as it cannot interfere with the formed stable compounds. However, MgO has an impact on the material of sinter in the immediate vicinity of the

interface, where it stabilizes magnetite, sometimes even to the spinel - magnesium ferrite mixture form [13]. Inner area (see dash line) in Figure 5 show evidence of etched Ca<sub>2</sub>Fe<sub>2</sub>O<sub>5</sub>, the granular structure is a result of MgO grains.

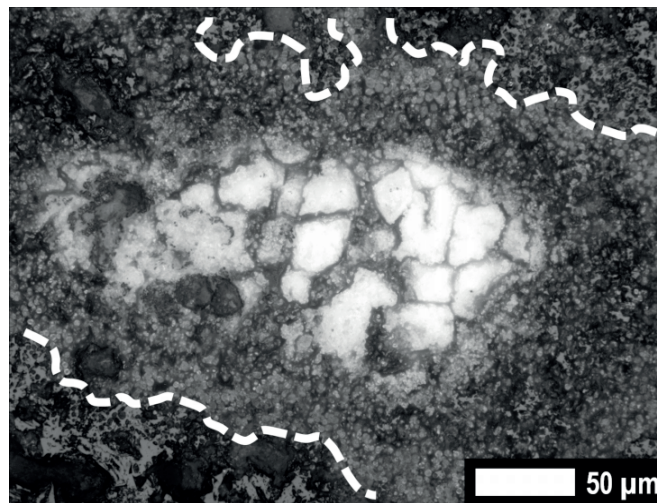


Fig. 5. The residue of dolomite in sinter after etching with 24.7 % HCl (LM)

#### 4.2. Calcium ferrites

In the group of calcium ferrites is mainly visible the increase of the content of Ca<sub>2</sub>Fe<sub>2</sub>O<sub>5</sub>. It is formed in the areas of the basic additives assimilation with the largest amount of the CaO donor. It is often embedded in the mono calcium ferrite matrix; however, it has not been recorded in diffraction records. Low values were observed just in case of Sample A1 and DU86 where there also is a high ratio of the residual phase from hematite ore – quartz, which confirms that increased ratios of dicalcium ferrite in other sinters are due to an increased rate of assimilation of basic additives. Although the ratios of another residual phase – dolomite seems to be well-balanced, these data are distorted by diffraction peaks of other phases which the dolomite phases overlap. The above-mentioned binary calcium ferrites are present in the samples with only a minimum of additives. The most common impurity of Ca<sub>2</sub>Fe<sub>2</sub>O<sub>5</sub> is usually SiO<sub>2</sub> (~ 9 %), substitution of Fe<sup>3+</sup> by Al<sup>3+</sup> cation is taken into account in Table 4 by data for brownmillerite. Monocalcium ferrite is usually present in a pure state.

Remarkable is the ratio of calcium ferrites in sample OS42. There is a majority share of Ca<sub>2</sub>Fe<sub>22</sub>O<sub>33</sub> ternary ferrite, the rational formula of which can be written as 2CaO·4FeO·9Fe<sub>2</sub>O<sub>3</sub>. So, in addition to trivalent iron it contains a significant amount of Fe<sup>2+</sup>. The crystal habitus corresponding to the Ca<sub>2</sub>Fe<sub>22</sub>O<sub>33</sub> composition is shown in Figure 6. In the performed EDX analysis (Table 6) the starting ratio of iron for this compound was in conversion divided according to the theoretical ratio of Fe<sup>2+</sup>/Fe<sup>3+</sup>.

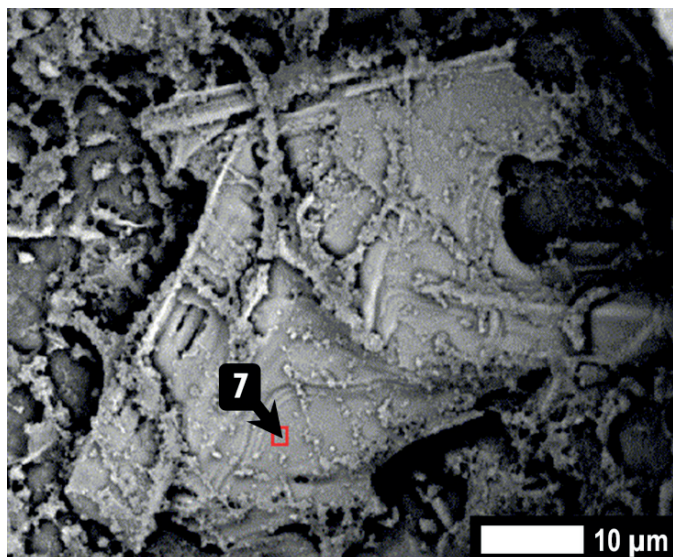


Fig. 6. Crystalline compound the content of which corresponds to  $\text{Ca}_2\text{Fe}_{22}\text{O}_{33}$  with ash from walnut shells and particles of  $\text{CaO}$  (SEM); 7 – see Table 6

In addition to binary and tertiary calcium ferrites the sinters also contain multicomponent ferrites, the unambiguous identification of which is often problematic and during the observation they are most often marked as silico-ferrites of calcium and aluminum. The research of these complex compounds is gaining momentum mainly recently and they are not present in the used diffraction databases, therefore also the ratio of calcium ferrites used for this research was established as a sum of ratios of all found calcium ferrites.

Most scientific studies on SFCA divide them into three groups designated SFCA, SFCA-I, and SFCA-II. The latter compound has specific chemical composition with a high content of  $\text{Al}_2\text{O}_3$  and was observed mainly in sinters of African ores [14]. Its presence was not identified even in the samples included in this study.

Based on research also the morphological shapes mainly related to thermal conditions for their formation were also assigned to the above-mentioned type of complex calcium ferrites. So SFCA-I is a low-temperature form originating in iron ore sinters at temperatures under  $1250\text{ }^\circ\text{C}$  with approximate composition of 84 %  $\text{Fe}_2\text{O}_3$ , 13 %  $\text{CaO}$ , 1 %  $\text{SiO}_2$  and 2 %  $\text{Al}_2\text{O}_3$ . According to the above it has the high-iron (low-silicon) attribute. In the cross section it forms needle-like crystals, so in most cases this type is designated as the acicular type [15]. The high-temperature form, SFCA, is supposed to be formed at temperatures above  $1300\text{ }^\circ\text{C}$ , but it also occurs in sinters sintered at lower temperatures. Chemical composition in the range of 60 % – 76 %  $\text{Fe}_2\text{O}_3$ , 13 – 16 %  $\text{CaO}$ , 3 – 10 %  $\text{SiO}_2$ , 4 – 10 %  $\text{Al}_2\text{O}_3$ , 0.7 – 1.5 %  $\text{MgO}$  gives to this type the low-iron high silicon attribute. Its typical morphology in the cross section is the columned morphology [16].

Although this definition of silico-ferrites of calcium and aluminum was adopted by several authors, during this study some of its shortcomings manifested themselves. These shortcomings were related to the morphological classification and Tonžetić and Dippenaar also pointed out to them [17]. The chemical composition of all found SFCA approximately corresponds to the above two groups with differences mainly

in the alumina content, which is in our case generally lower. Mean composition of the analyzed SFCA in case of all types of sinters is shown in Table 5. Although [17] speak of frequent absence of  $\text{Al}_2\text{O}_3$  in SFCA-I, in all analyzed cases the presence of aluminum was confirmed in the EDX spectrum (an example is shown in Figure 8). Even though SFCA can also contain  $\text{Fe}^{2+}$  [18], for the needs of this study iron was converted as  $\text{Fe}_2\text{O}_3$ .

TABLE 5  
Mean composition of found SFCA and SFCA-I

Modification	Oxide ratio [wt %]				
	$\text{Fe}_2\text{O}_3$	$\text{CaO}$	$\text{SiO}_2$	$\text{Al}_2\text{O}_3$	$\text{MgO}$
SFCA	68	17	10	2	1
SFCA-I	80	12	4	1.5	1

As all types of SFCA form longitudinal habits, according to [19], the limit boundary between both types is the size of the cross section perpendicular to the longer side of crystals –  $10\text{ }\mu\text{m}$ . According to this criterion, during the phase composition quantification by counting points on LM, the SFCA and SFCA-I mix-up may occur. The reason is the fact that both SFCA-I and SFCA are composed of plate crystals in the thickness from approximately  $1\text{ }\mu\text{m}$ . The proofs are the plates, identical in shape, in the pore, shown in Figure 3 where SFCA-I and SFCA are alternately crystallized while the analyzed crystal in Table 3 under number 4 is exactly the low-iron form. Thicker high-iron SFCA-I are shown in Figure 4 under number 5. The thickness of this crystal in the cross section is approximately  $10\text{ }\mu\text{m}$ .

The difference in chemical composition of both ferrite modifications is reflected in their density, which is the main factor affecting reflectiveness of light. Thus, in visual terms both types can be distinguished microscopically but this difference is very small and requires the contrast to be set very carefully on light microscope. Therefore using the SEM-EDX technology for identification is the most reliable method, as cited by [17].

It resulted from the further study of SFCA a SFCA-I on the sinter samples that these compounds not only coexist side-by-side but also intergrows each other very often. Just in such cases their distinction is very difficult, especially when magnetite is also included in the intergrowing. Its shade of gray makes it most similar to SFCA. Figure 7 shows all 3 phases with the morphology differentiation. Visible pores result from natural porosity, by dark or etched silicates (the sample was previously etched with HF, the effect of which remained at a certain depth even after grinding, mainly in case of  $\text{Ca}_2\text{SiO}_4$ ).

Crystals on the left bottom in the Figure 7, in the thickness of  $5\text{ }\mu\text{m}$ , which would at morphological classification seem to be SFCA-I, are in fact intergrowths of both types of SFCA. As the microstructure of sinters where the main bonding phase consists of the so-called acicular calcium ferrites is because of its strength and metallurgical properties considered to be the ideal microstructure [19], it is appropriate to ask a question whether these ferrites could be considered exclusively as SFCA-I, when the presented findings confirm analogical morphology for both modifications and thus the presence of low-iron SFCA in fields formed by the calcium ferrite needles. The intergrowing and coexistence of SFCA and SFCA-I is

clearly visible also in the study by Sacramento de Magalhães and Roberto Gomes Brandão [20]. These authors consider SFCA to be a pseudomorph of magnetite. SFCA formation with contribution of magnetite grains is considered also by the authors in [21], with a reference to increased contents of MgO in the analyzed ferrites.

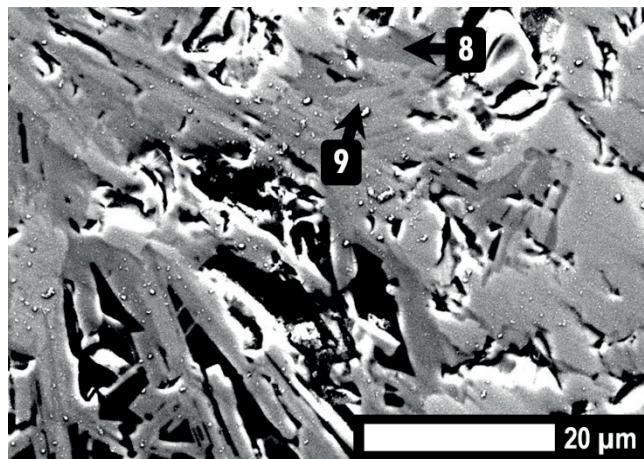


Fig. 7. SFCA and SFCA-I intergrowths (SEM); M – magnetite, F – SFCA, F-I – SFCA-I, S/P – silicates/pores, 8, 9 – see Table 6

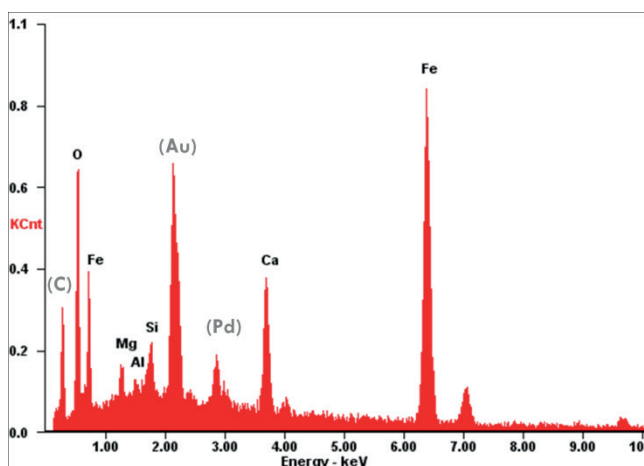


Fig. 8. EDX spectrum for Point 9 (SFCA-I)

EDX analyses of intergrowths from Figure 7 are shown in Table 6. Also in this case a higher MgO content was observed

for SFCA; however for SFCA-I the MgO content is even higher and even at the overall comparison of two types of found complex calcium ferrites the one with a higher magnesium ratio cannot be clearly identified.

TABLE 6

EDX analysis of selected points after conversion to oxides

#	Oxide ratio [wt %]						
	Fe <sub>2</sub> O <sub>3</sub>	CaO	SiO <sub>2</sub>	Al <sub>2</sub> O <sub>3</sub>	MgO	Na <sub>2</sub> O	FeO
7*	71.9	8.5	2.8	0.7	-	-	16.0
8	69.0	16.8	11.6	0.8	1.4	0.5	-
9	83.7	9.8	3.7	0.5	2.3	-	-

\*iron converted according to theoretical ratio of Fe<sup>2+</sup>/Fe<sup>3+</sup>; for other cases it is considered as Fe<sup>3+</sup>

### 4.3. Silicates

Also the ratio of silicates in respective samples is according to Table 4 proportional to the conditions for formation of secondary phases, therefore the greatest values are again in case of sinters prepared with an additive of walnut shells. Larnite, also with respect to its enormous thermodynamic stability, maintains its main role in this group of mineral phases. It is rarely in a completely pure state, it contains mainly isomorphous additives of FeO. Similarly to Ca<sub>2</sub>SiO<sub>4</sub>, sinters A1, DU44 and DU86 contain also hedenbergite CaFeSi<sub>2</sub>O<sub>6</sub> belonging to inosilicates. Its presence is visible mainly in the areas with occurrence of glass where it is crystallized in a dendritic form in the glass matrix. However, small crystals are arranged next to each other so closely that the glass content is reduced in such areas to a minimum. The view of a hedenbergite field is shown in Figure 9. Phases etched with hydrochloric acid are very good visible, black area represents the fully etched amorphous phase.

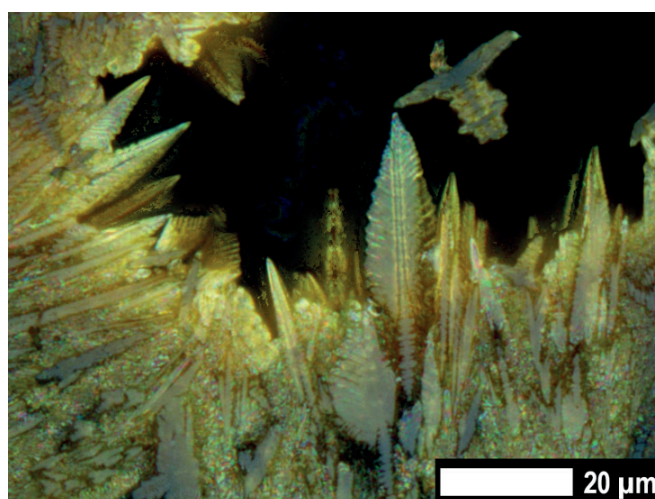


Fig. 9. Dendrites of hedenbergite after etching with 24.7 % HCl (LM)

Another inosilicate phase – wollastonite CaSiO<sub>3</sub> proved to be problematic. Apart from the areas with glass, i.e. there where the melt solidified as the last one, its occurrence is associated with intergranular dendrites of iron oxides which define the habitus shape on the edges of CaSiO<sub>3</sub> as shown in Figure 10.

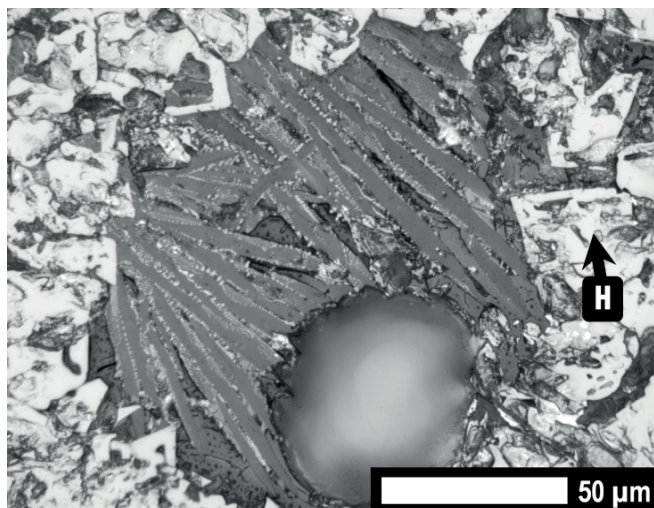


Fig. 10. Association of hematite and wollastonite after etching with 3% HNO<sub>3</sub> (LM)

Wollastonite frequently behaves as dicalcium silicate – it crystallizes directly between SFCA and forms with them a very tight association and thereby often affects their shape. Its quantification by the X-Ray diffraction analysis was a problem. Although under light microscope its significant ratio can be clearly seen but in the sinter that is a very heterogeneous system, diffraction lines of other phases interfere with diffraction peaks of CaSiO<sub>3</sub> and thus make impossible their easy identification. Therefore, the data in Table 4 may also be distorted as the phase itself was added to the evaluation only later.

#### 4.4. Iron oxides

The phases that are most frequently represented in the studied samples are iron oxides which are partly reduced during the sintering process but also largely participate in the formation of other compounds, mainly calcium ferrites as the sinters in question are produced with the basicity ~ 1.6.

Extreme cases are again represented by sample A1 and DU86 where the ratio of hematite is substantially higher. This should be attributed to the high content of primary hematite in the unreacted lumps of hematite ore as evidenced by high silica contents. The following three forms of hematite are identified in sinter: primary, secondary, and tertiary (martitic) form [22]. They differ only in the manner of their origin but not in their chemical composition or parameters of their crystal lattice, so they cannot be separately identified using the X-Ray diffraction analysis. The found hematite was usually pure, which is in agreement with his slightly vacant lattice where it is very difficult for foreign atoms to diffuse in. Except for A1 and DU86, Fe<sub>2</sub>O<sub>3</sub> maintained its approximately 20 % level in all other samples. The view of the set of the hematite subhedral crystals is shown in Figure 11.

Magnetite has a ratio that is by approximately 10 % higher, but only in case of DU44 and OS35. The reasons for the larger ratio of Fe<sub>2</sub>O<sub>3</sub> than Fe<sub>3</sub>O<sub>4</sub> in sinters A1 and DU86 have already been explained. Despite an advanced assimilation of primary phases also occurred in sinter OS42, here the magnetite ratio remained behind, at the value of almost 20 %. As because of

that there was also no increase in the hematite ratio, the cause must be searched for in other groups – in case of silicates no extreme value was observed but the content of calcium ferrites increased by almost 14 % compared to the amount in sample OS35, which is almost the exact difference between sample OS35 and OS42 in ratios of magnetite. As already mentioned in case of calcium ferrites, there was a radical increase of mainly ternary calcium ferrites Ca<sub>2</sub>Fe<sub>22</sub>O<sub>33</sub>. This is the explanation of the occurring FeO·Fe<sub>2</sub>O<sub>3</sub> deficit that was stabilized in structure 2CaO·4FeO·9Fe<sub>2</sub>O<sub>3</sub>.

All values for magnetite shown in Table 4 are defined in diffractograms for Fe<sup>2+</sup>Fe<sup>3+</sup><sub>2</sub>O<sub>4</sub> and do not take into account different chemical composition of real magnetite grains. Because of its defective lattice magnetite tends to take up foreign cations, which applies mostly for Mg<sup>2+</sup>. Magnesium ferrite (Mg,Fe)Fe<sub>2</sub>O<sub>4</sub> spinel usually prevails in the regions with dolomite residues and magnetite with significant presence of CaO–(Fe,Ca,Mg)Fe<sub>2</sub>O<sub>4</sub>, also referred to as calciomagnetite, is also wide-spread [17,23].

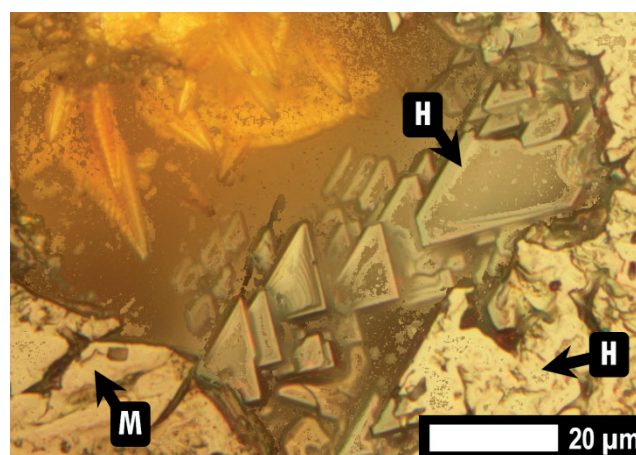


Fig. 11. Crystals of secondary hematite, magnetite, and dendritic hedenbergite after etching glass with 24.7 % HCl (LM) H – hematite, M - magnetite

## 5. Conclusions

Replacement of part of coke breeze in the sinter mixture with the biomass-based fuels changes the sintering conditions, which leads to the change in ratio of some phases. However, these changes are due to the changed temperature profile and not to the chemical composition of alternative fuels, the mineral matters of which are of a significant basic nature. The only difference in the local microstructure where the fuel grain were present, are non assimilated ash particles forming chain clusters in case of charcoal and network fibers in case of walnut shells. Potassium compounds were not observed in the samples despite their high occurrence declared by external analyses of the wood biomass ashes. When comparing the phase composition of individual sinters there is a direct correlation visible between the ratio of phases when higher quartz volumes result in also higher volumes of hematite which is part of the unreacted ore. Moreover, a higher rate of assimilation also resulted in increased volumes of calcium ferrites along with silicates. High ratio of tertiary calcium ferrite Ca<sub>2</sub>Fe<sub>22</sub>O<sub>33</sub> in the sample prepared with walnut shells

as a substitute of coke - OS42 - was anomal; it was due to the stabilization of magnetite in the structure of this ferrite. Also a intergrowing and coexistence of two modifications of silico-ferrites of calcium and aluminum – high-iron and low-iron form, the morphology of which proved to be insufficient criterion for their correct identification, was observed in the sinters. Finally, it can be concluded that the implementation of studied fuels in the sinter mixture had no negative impact on the phase composition of the produced sinters, which therefore confirms its prospective application in the sintering process.

#### Acknowledgements

This work was supported by Slovak Research and Development Agency (APVV), Slovak Republic, No. APVV-0405-11 and VEGA 1/0475/13

Authors thanks the U. S. Steel Košice, s.r.o. Research & Development employees for the provided services, namely Jana Godlová, Jana Kuchtová and Anna Vargová for sample preparation, Slávka Hockicková, Marta Šohajová, Erika Janočková and Lucia Hrabčáková for SEM-EDX analyses and Peter Vranec for XRD analyse.

#### REFERENCES

- [1] M. Fröhlichová, R. Findorák, J. Legemza, Archives of Metallurgy and Materials 58, 179 – 185 (2013).
- [2] T. Norgate, N. Haque, M. Somerville, S. Jahanshahi, ISIJ International 52, 1472 – 1481 (2012).
- [3] T.G. Bridgeman, J.M. Jones, I.Shield, P.T. Williams, Fuel 87, 844 – 856 (2008).
- [4] M. Fröhlichová, J. Legemza, R. Findorák, A. Mašlejová, Archives of Metallurgy and Materials 59, 815 – 820 (2014).
- [5] R.R. Lovel, K.R. Vining, M.Dell'Amico, ISIJ International 49, 195 – 202 (2009).
- [6] M. Gan, X. Fan, X. Chen, Z. Ji, W. Lv, Y. Wang, Z. Yu, T. Jiang, ISIJ International 52, 1574 – 1578 (2012).
- [7] L. Lu, M. Adam, M. Kilburn, S. Hapugoda, M. Somerville, S. Jahanshahi, J.G. Mathieson, ISIJ International 53, 1607 – 1616 (2013).
- [8] T. Ya. Malysheva, Yu. S. Yusfin, N.R. Mansurova, M.F. Gibadulin, V. P. Lekin, Steel in Translation 37, 129 – 130 (2007).
- [9] F. Zhang, S. An, G. Luo, Y. Wang, Journal of Iron and Steel Research, International 19, 1 – 5, (2012).
- [10] J. Legemza, M. Fröhlichová, R. Findorák, F. Bakaj, Acta Metallurgica Slovaca 17, 245 – 252 (2011).
- [11] M. Grigore, R. Sakurovs, D. French, V. Sahajwalla, ISIJ International 47, 62 – 66 (2007).
- [12] S.V. Vassilev, D. Baxter, L.K. Andersen, C.G. Vassileva, Fuel 105, 40 – 76 (2013).
- [13] K. Higuchi, T. Tanaka, T. Sato, ISIJ International 47, 669 – 678 (2007).
- [14] T. van den Berg, An assessment of the production of fine material in iron ore sinter. MSc Dissertation, University of Pretoria, Pretoria (2008).
- [15] W.G. Mumme, J.M.F. Clout, R.W. Gable, Neues Jahrb. Miner. Abh. 173, 93 – 117 (1998).
- [16] S.N. Ahsan, T. Mukherjee, J.A. Whiteman, Ironmaking Steelmaking 10, 56 – 64 (1983).
- [17] I. Tonžetić, A. Dippenaar, Minerals Engineering 24, 1258 – 1263 (2011).
- [18] N.A.S. Webster, M.I. Pownceby, I.C. Madsen, J.A. Kimpton, ISIJ International 53, 774 – 781 (2013).
- [19] A. Cores, A. Babich, M. Muñoz, S. Ferreira, J. Mochon, ISIJ International 50, 1089 – 1098 (2010).
- [20] M. Sacramento de Magalhães, P. Roberto Gomes Brandão, Minerals Engineering 16, 1251 – 1256 (2003).
- [21] T. Ya. Malysheva, M. F. Gibadulin, N.R. Mansurova, V. P. Lekin, Russian Metallurgy (Metally), 169 – 172 (2007).
- [22] S.C. Panigrahy, P. Verstraeten, J. Dilewijns, Metallurgical Transactions 15, 23-32 (1984).
- [23] <http://www.iron-consortium.org>

Received: 20 October 2014.

